Chiral extrapolation of the doubly charmed baryons magnetic properties

Jiong-Jiong Liu,[1,2,3] Zhan-Wei Liu,[1,2,3,*] Xiu-Lei Ren,[4,5,†] and Yu Zhuge[1,2,3]

[1]*School of Physical Science and Technology, Lanzhou University, Lanzhou 730000, China*
[2]*Research Center for Hadron and CSR Physics, Lanzhou University and Institute of Modern Physics of CAS, Lanzhou 730000, China*
[3]*Lanzhou Center for Theoretical Physics, MoE Frontiers Science Center for Rare Isotopes, Key Laboratory of Quantum Theory and Applications of MoE, Key Laboratory of Theoretical Physics of Gansu Province, Gansu Provincial Research Center for Basic Disciplines of Quantum Physics, Lanzhou University, Lanzhou 730000, China*
[4]*School of Nuclear Science, Energy and Power Engineering, Shandong University, Jinan 250061, China*
[5]*Helmholtz Institut Mainz, D-55099 Mainz, Germany*

(Received 27 March 2025; accepted 19 June 2025; published 30 June 2025)

The magnetic moments, magnetic form factors, and transition magnetic form factors of doubly charmed baryons are studied within heavy baryon chiral perturbation theory. We regulate the loop integrals using the finite-range regularization. The contributions of vector mesons are taken into account to investigate the dependence of form factors on the transferred momentum. The finite volume and lattice spacing effects are considered to analyze the lattice QCD simulations which can be understood well in our framework.

DOI: 10.1103/gknb-p56r

I. INTRODUCTION

The physics of heavy flavor hadrons has been developing with great experimental progress and exhibited special characters due to the large masses of heavy quarks. The doubly charmed baryons have been searched for by various experimental collaborations [1–12]. The SELEX Collaboration reported results for Ξ_{cc}^{+} in 2002 [13], and the LHCb Collaboration reported evidence for Ξ_{cc}^{++} in 2017 [14].

The structure of these heavy flavor hadrons is important for us to understand the nonperturbative behavior of QCD. In addition to the mass spectra and strong decays, the electromagnetic form factors are indispensable tools for exploring the property of doubly charmed baryons [15–22]. The magnetic moments of doubly charmed baryons were studied by utilizing the quark model since the 1970s [23], and it has been further investigated with different quark models [24–41], MIT bag model [42–45], Skyrmion model [46], light-cone QCD sum rule [47], and so on [48–52].

The transition magnetic form factors connect both ground and excited doubly charmed baryons and play important roles in the radiative decays and other properties. The radiative decays of doubly charmed baryons have been studied in the MIT bag model [44,53,54], the quark model [32], light-cone QCD sum rule [55–58], and so on [48–50,59–63]. The magnetic moments and the transition magnetic moments were discussed within the heavy baryon chiral perturbation theory (HBChPT) [64–66].

Significant advancements have been taken with the lattice QCD over the past decade, and some lattice QCD collaborations have simulated the electromagnetic factors of doubly charmed baryons [67–71]. In addition, the magnetic moments and form factors have been further investigated in the extended on-mass-shell scheme by analyzing lattice QCD results [72,73], and the similar analysis for the transition ones would also be very helpful.

In this work, we use the unified framework to study both the magnetic form factors $G_M(q^2)$ and transition magnetic form factors $G_{M1}(q^2)$ as well as their relevant moments. We study the above quantities from lattice QCD with HBChPT, and finite-volume (FV) effect and lattice spacing correction are specially included and carefully examined. We consider the one-loop contributions and discuss the effects of excited doubly charmed baryons on the magnetic moments of ground ones. Vector mesons are also involved for nonzero q^2.

Besides the dimensional regularization, we also employ an alternative finite-range regularization (FRR) to calculate those loop integrals which occur in the HBChPT [74,75]. Since the numerical results of these two regularization methods differ very much [74,75], it is important to check whether they are both consistent with the current lattice QCD data. Moreover, the latter regularization is more convenient to study the effect of finite volume.

*Contact author: liuzhanwei@lzu.edu.cn
†Contact author: xiulei.ren@uni-mainz.de

There are three parts in the transition magnetic form factors $G_{M1}(q^2)$, and the G_3 relevant terms were ignored when the photon is on shell for the radiative decays of singly heavy baryons and doubly charmed baryons [64,76]. As in the $N \to \Delta$ transition process, the G_3 terms would also contribute to the $G_{M1}(0)$ [77–81]. We will study these terms and investigate their roles in the doubly charmed baryon system.

This paper is organized as follows. In Sec. II, we present the contributing effective Lagrangians at $\mathcal{O}(p^2)$. In Sec. III, the magnetic moments and form factors are studied within HBChPT. The finite-range regularization is used to deal with the loop integrals. The finite-volume and lattice spacing effects are considered. The contributions of vector mesons are introduced to form factors $G_M(q^2)$. In Sec. IV, we extrapolate the $G_{M1}(q^2)$ up to $\mathcal{O}(p^3)$ in a similar way with the help of the lattice results. A short summary follows in Sec. V.

II. EFFECTIVE LAGRANGIANS

We present the relevant chiral Lagrangians in HBChPT following Refs. [64,65,82]. The spin-$\frac{1}{2}$ doubly charmed baryon fields are collected in [83,84]

$$\Psi = \begin{pmatrix} \Xi_{cc}^{++} \\ \Xi_{cc}^{+} \\ \Omega_{cc}^{+} \end{pmatrix} \Rightarrow \begin{pmatrix} ccu \\ ccd \\ ccs \end{pmatrix}, \tag{1}$$

the spin-$\frac{3}{2}$ doubly charmed baryon fields are denoted by the Rarita-Schwinger fields as [85]

$$\Psi^{*\rho} = \begin{pmatrix} \Xi_{cc}^{*++} \\ \Xi_{cc}^{*+} \\ \Omega_{cc}^{*+} \end{pmatrix}^{\rho} \Rightarrow \begin{pmatrix} ccu \\ ccd \\ ccs \end{pmatrix}^{\rho}, \tag{2}$$

and the pseudoscalar meson fields are introduced as

$$\phi = \begin{pmatrix} \pi^0 + \frac{1}{\sqrt{3}}\eta & \sqrt{2}\pi^+ & \sqrt{2}K^+ \\ \sqrt{2}\pi^- & -\pi^0 + \frac{1}{\sqrt{3}}\eta & \sqrt{2}K^0 \\ \sqrt{2}K^- & \sqrt{2}\bar{K}^0 & -\frac{2}{\sqrt{3}}\eta \end{pmatrix}. \tag{3}$$

We choose the nonlinear realization of the chiral symmetry,

$$U = u^2 = \exp(i\phi/f_\phi), \tag{4}$$

and f_ϕ denote the decay constant of pseudoscalar meson, and $f_\pi = 92.4$ and $f_K = 113$ MeV are used in this work. The chiral axial vector field is defined as [82]

$$u_\mu = \frac{1}{2} i[u^\dagger(\partial_\mu - ir_\mu)u - u(\partial - il_\mu)u^\dagger], \tag{5}$$

where $r_\mu = l_\mu = -eQA_\mu$, and $Q = \mathrm{diag}\,(2/3, -1/3, -1/3)$ for the pure meson Lagrangians while $Q = \mathrm{diag}\,(2, 1, 1)$ for baryon fields.

In HBChPT, the charmed baryon fields Ψ can be decomposed into the large component H and the small one L,

$$H = e^{im_B v\cdot x}\frac{1+\not{v}}{2}\Psi, \qquad L = e^{im_B v\cdot x}\frac{1-\not{v}}{2}\Psi, \tag{6}$$

where $v_\mu = (1, \vec{0})$ is the velocity of the baryon. The momentum is decomposed as $p^\mu = m_B v^\mu + k^\mu$, and thus k^μ is a small quantity. The HBChPT Lagrangians are obtained from the relativistic Lagrangians after the above separation. In this work, the contribution from small components is beyond the accuracy we consider currently. We use B and T to denote the large components of spin-$\frac{1}{2}$ and spin-$\frac{3}{2}$ doubly charmed baryons. The difference of the mass is denoted $\delta = m_T - m_B$ which appears in the propagators.

The relativistic Lagrangian at $\mathcal{O}(p^2)$ contributing to the magnetic moments of doubly charmed baryons at the tree level reads

$$\mathcal{L}^{(2)}_{\gamma BB} = \frac{a_1}{8m_B}\bar{\Psi}\sigma^{\mu\nu}\hat{F}^+_{\mu\nu}\Psi + \frac{a_2}{8m_B}\bar{\Psi}\sigma^{\mu\nu}\Psi\mathrm{Tr}(F^+_{\mu\nu}), \tag{7}$$

where $a_{1,2}$ are the low-energy constants, and the traceless operator $\hat{F}^+_{\mu\nu} = F^+_{\mu\nu} - \frac{1}{3}\mathrm{Tr}(F^+_{\mu\nu})$. The chirally covariant QED field strength tensor $F^+_{\mu\nu} = u^\dagger F^R_{\mu\nu}u + uF^L_{\mu\nu}u^\dagger$, where $F^R_{\mu\nu} = \partial_\mu r_\nu - \partial_\nu r_\mu - i[r_\mu, r_\nu]$ and $F^L_{\mu\nu} = \partial_\mu l_\nu - \partial_\nu l_\mu - i[l_\mu, l_\nu]$. After the nonrelativistic reduction, the HBChPT Lagrangian is

$$\mathcal{L}^{(2)}_{\gamma BB} = a_1\frac{-i}{4m_B}\bar{B}[S^\mu, S^\nu]\hat{F}^+_{\mu\nu}B + a_2\frac{-i}{4m_B}\bar{B}[S^\mu, S^\nu]B\mathrm{Tr}(F^+_{\mu\nu}), \tag{8}$$

and the $\mathcal{O}(p^2)$ tree-level terms which contribute to the spin-$\frac{1}{2}$ to spin-$\frac{3}{2}$ transition magnetic moment are

$$\mathcal{L}^{(2)}_{\gamma BT} = a_3\frac{-i}{2m_B}\bar{T}^\mu\hat{F}^+_{\mu\nu}S^\nu B + a_4\frac{-i}{2m_B}\bar{T}^\mu S^\nu B\mathrm{Tr}(F^+_{\mu\nu}) + \mathrm{H.c.} \tag{9}$$

The $\mathcal{O}(p^2)$ pure meson Lagrangian is

$$\mathcal{L}^{(2)}_{\gamma MM} = \frac{f_0^2}{4}\mathrm{Tr}[\nabla_\mu U(\nabla^\mu U)^\dagger], \tag{10}$$

with $\nabla_\mu U = \partial_\mu U - ir_\mu U + iUl_\mu$.

The Lagrangian which describes the interaction of vector mesons and photons is given by [73,86]

$$\mathcal{L}_\gamma = -\frac{1}{2\sqrt{2}}\frac{F_V}{m_V}\mathrm{Tr}[V_{\mu\nu}F^{+\mu\nu}], \tag{11}$$

where F_V is the decay constant of $V \to e^+e^-$ and $V_{\mu\nu} = \partial_\mu V_\nu - \partial_\nu V_\mu$ with

$$V_\mu = \begin{pmatrix} \frac{1}{\sqrt{2}}\rho^0 + \frac{1}{\sqrt{2}}\omega & \rho^+ & K^{*+} \\ \rho^- & -\frac{1}{\sqrt{2}}\rho^0 + \frac{1}{\sqrt{2}}\omega & K^{*0} \\ K^{*-} & \bar{K}^{*0} & \phi \end{pmatrix}_\mu . \tag{12}$$

The $\mathcal{O}(p^1)$ Lagrangian describing the interaction between two baryons and a pseudoscalar meson reads

$$\mathcal{L}^{(1)}_{\mathrm{int}} = \frac{\tilde{g}_A}{2}\bar{\Psi}\not{u}\gamma_5\Psi + \frac{\tilde{g}_B}{2}\bar{\Psi}^{*\mu}g_{\mu\nu}\not{u}\gamma_5\Psi^{*\nu} + \frac{\tilde{g}_C}{2}[\bar{\Psi}^{*\mu}u_\mu\Psi + \bar{\Psi}u_\mu\Psi^{*\mu}]. \tag{13}$$

The corresponding nonrelativistic form is written as

$$\mathcal{L}^{(1)}_{\mathrm{int}} = \tilde{g}_A\bar{B}S^\mu u_\mu B + \tilde{g}_B\bar{T}^\rho S^\mu u_\mu T_\rho + \frac{\tilde{g}_C}{2}[\bar{T}^\mu u_\mu B + \bar{B}u_\mu T^\mu]. \tag{14}$$

To investigate the impact of vector mesons on the magnetic form factors and transition form factors, we refer to Ref. [73] for the following Lagrangians within the HBChPT framework:

$$\mathcal{L}_{VBB} = -\frac{ig_V}{2m_B}\bar{B}[S^\mu, S^\nu]V_{\nu\mu}B, \tag{15}$$

$$\mathcal{L}_{VBT} = -\frac{i\sqrt{3}d_V}{2m_B}\bar{T}^\mu V_{\mu\nu}S^\nu B. \tag{16}$$

Utilizing the heavy quark symmetry, the spin-$\frac{1}{2}$ and spin-$\frac{3}{2}$ states can be unified in a superfield [87,88],

$$\psi^\mu = T^\mu - \sqrt{\frac{1}{3}}(\gamma^\mu + v^\mu)\gamma_5 B. \tag{17}$$

With the Lagrangian $\kappa\bar{\psi}^\mu\not{u}\gamma_5\psi_\mu$ describing the interaction between two baryons and a pseudoscalar meson [76], one can obtain the relations for the pseudoscalar couplings in Eq. (14):

$$\tilde{g}_B = 3\tilde{g}_A, \qquad \tilde{g}_C = 2\sqrt{3}\tilde{g}_A. \tag{18}$$

Similarly, the vector couplings satisfy the following relation from the Lagrangian $\frac{i\kappa_V}{m_B}\bar{\psi}^\mu V_{\mu\nu}\psi^\nu$:

$$d_V = g_V. \tag{19}$$

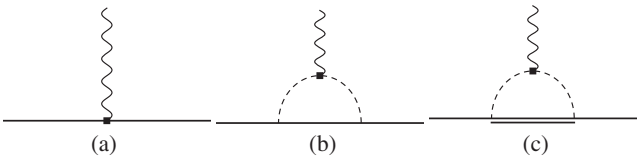

FIG. 1. Feynman diagrams contributing to the magnetic moment up to $\mathcal{O}(p^3)$ level. The single (double) solid lines refer to the spin-$\frac{1}{2}$ (spin-$\frac{3}{2}$) baryons, and dashed and wavy lines represent the mesons and photons.

III. MAGNETIC MOMENTS AND FORM FACTORS

A. Magnetic moments

In HBChPT, the matrix elements of the electromagnetic vector current for spin-$\frac{1}{2}$ heavy baryon is defined as

$$\langle\Psi(p')|J_\mu|\Psi(p)\rangle = e\bar{u}(p')\mathcal{O}_\mu(p', p)u(p). \tag{20}$$

After obtaining the nonrelativistic limit Lagrangians, the tensor $\mathcal{O}_\mu$ can be expressed as

$$\mathcal{O}_\mu(p', p) = v_\mu G_E(q^2) + \frac{[S_\mu, S_\nu]q^\nu}{m_B}G_M(q^2). \tag{21}$$

The magnetic moment and magnetic radii can thus be extracted,

$$\mu_B = \frac{e}{2m_B}G_M(0), \quad \langle r^2_M\rangle = \frac{6}{G_M(0)}\frac{dG_M(q^2)}{dq^2}\bigg|_{q^2=0}. \tag{22}$$

There are three Feynman diagrams contributing to the magnetic moments up to order $\mathcal{O}(p^3)$ in Fig. 1. We also investigated the impact of spin-$\frac{3}{2}$ doubly charmed baryons as the intermediate states through the diagram Fig. 1(c). The relevant Lagrangians are listed in Sec. II. The tree-level diagram comes from the Lagrangian in Eq. (7) which has two couplings a_1, a_2. The loop diagrams contain the meson-meson-photon vertices described by Eq. (10) and baryon-baryon-meson vertices with three couplings $\tilde{g}_A$, $\tilde{g}_B$, and $\tilde{g}_C$ as in Eq. (14). Within the heavy quark limit as detailed in Sec. II, the three coupling constants $\tilde{g}_A$, $\tilde{g}_B$, and $\tilde{g}_C$ exhibit well-defined proportionality relations, $\tilde{g}_B = 3\tilde{g}_A$ and $\tilde{g}_C = 2\sqrt{3}\tilde{g}_A$. We adopt the value $\tilde{g}_A = -0.4$ obtained with the heavy antiquark diquark symmetry as reported in Refs. [72,73,89].[1] When the charm quarks are treated as noninteracting spectators in the quark model, the derived coupling relations show agreement with those predicted by the heavy quark limit.

The tree-level expression of the magnetic moment is summarized in Table I and the loop correction is

[1]The $\tilde{g}_A$ in Refs. [72,73] differs from ours by a factor 2, which arises from a different definition of the u_μ in Eq. (5).

TABLE I. The doubly charmed baryons magnetic moments at the tree level.

μ	Tree-level expression
Ξ_{cc}^{++}	$\frac{e}{m_{\Xi_{cc}^{++}}}(\frac{1}{3}a_1+2a_2)$
Ξ_{cc}^{+}	$\frac{e}{m_{\Xi_{cc}^{+}}}(-\frac{1}{6}a_1+2a_2)$
Ω_{cc}^{+}	$\frac{e}{m_{\Omega_{cc}^{+}}}(-\frac{1}{6}a_1+2a_2)$

$$\mu_B^{(2,\mathrm{loop})} = \sum_{\phi,i}\frac{e\zeta^{(\phi,i)}\tilde{g}_i^2}{2f_\phi^2}n_3^{\mathrm{III}}|_{q^2\to 0} = \sum_{\phi,i}\frac{e\zeta^{(\phi,i)}\tilde{g}_i^2}{2f_\phi^2}\frac{-2I_0\omega - J_0 + (-2m^2+2\omega^2)L_0}{8}, \tag{23}$$

where the $\zeta^{(\phi,i)}$ is listed in Table II. The loop integrals like n_3^{III} are defined in the Appendix. When substituting the forms of loop integrals using dimensional regularization into Eq. (23), one can obtain the same results as in Ref. [65].

In the discussion below, the momentum-space cutoff is employed to remove the spurious high-energy physics. The contribution of high energies is encoded in the low-energy constants of the local chiral Lagrangian. We use the simple covariant dipole form factor to regulate the contribution integrals [75,90],

$$\left(\frac{-\Lambda^2}{l^2-\Lambda^2+i\epsilon}\right)^2. \tag{24}$$

For example, the integral $J_0(\omega)$ involving one meson and one baryon is regularized as

$$\begin{aligned} J_0(\omega) &= i\int\frac{d^4l}{(2\pi)^4}\frac{1}{(l^2-m^2+i\epsilon)(v\cdot l+\omega+i\epsilon)} \\ &\to i\int\frac{d^4l}{(2\pi)^4}\frac{1}{(l^2-m^2+i\epsilon)(v\cdot l+\omega+i\epsilon)}\left(\frac{-\Lambda^2}{l^2-\Lambda^2+i\epsilon}\right)^2 \\ &= \frac{-1}{16\pi^3}\int d^3\vec{l}\frac{1}{\vec{l}^2+m^2-\omega\sqrt{\vec{l}^2+m^2}}\left(\frac{\Lambda^2}{\vec{l}^2+\Lambda^2}\right)^2. \end{aligned} \tag{25}$$

TABLE II. The coefficients of the loop correction in Eq. (23).

	$\zeta^{(\pi,A)}$	$\zeta^{(K,A)}$	$\zeta^{(\pi,C)}$	$\zeta^{(K,C)}$
Ξ_{cc}^{++}	1	1	$-\frac{1}{3}$	$-\frac{1}{3}$
Ξ_{cc}^{+}	−1	0	$\frac{1}{3}$	0
Ω_{cc}^{+}	0	−1	0	$\frac{1}{3}$

When $\omega\to 0$, the above loop integral is written as

$$J_0(\omega\to 0) = \frac{-\Lambda^3}{16\pi(\Lambda+m)^2}, \tag{26}$$

which can be expanded in powers of $1/\Lambda$,

$$J_0(\omega\to 0) = -\frac{\Lambda}{16\pi}+\frac{m}{8\pi}+\mathcal{O}(\Lambda^{-1}). \tag{27}$$

This result is consistent with the one in d-dimensional regularization,

$$J_0(\omega\to 0) = 4\omega L(\lambda)+\frac{m}{8\pi}, \tag{28}$$

with the well-known ultraviolet divergence $L(\lambda) = \frac{\lambda^{(4-d)}}{16\pi^2}\{\frac{1}{d-4}-\frac{1}{2}[\ln(4\pi)+1+\Gamma'(1)]\}$ and the renormalization scale λ. In this special case, there is no chiral log terms. If taking a little complicated case $J_0(\omega\to -m)$ as an example,

$$J_0(\omega\to -m) = \frac{(m^2\pi-2m\Lambda-\pi\Lambda^2)\Lambda}{16\pi^2(\Lambda^2-m^2)} + \frac{m\Lambda(2\Lambda^2-m^2)\log\left(\frac{\Lambda+\sqrt{\Lambda^2-m^2}}{m}\right)}{8\pi^2(\sqrt{\Lambda^2-m^2})^3}, \tag{29}$$

where the nonanalytic log term is retained in the finite-range regularization. Furthermore, we can check that $J_0(\omega\to -m)$ can give the exact same $m\log m^2$ terms as the one in dimensional regularization when Λ is large enough:

$$\begin{aligned} J_0(\omega\to -m) &\overset{\mathrm{FRR}}{\to} \frac{-\Lambda}{16\pi}-\frac{m}{8\pi^2}\log\left(\frac{m^2}{4\Lambda^2/\mathrm{e}}\right)+\mathcal{O}(\Lambda^{-1}), \\ &\overset{\mathrm{DR}}{\to} 4\omega L(\lambda)-\frac{m}{8\pi^2}\log\left(\frac{m^2}{\lambda^2\mathrm{e}}\right). \end{aligned} \tag{30}$$

B. The finite-volume effect

In order to study the lattice QCD simulations, we need to consider the finite-volume effects. To introduce the finite-volume effects, the allowed three-dimensional momentum in the loop integrals is discretized,

$$\vec{l}_{\vec{n}} = \frac{2\pi}{L}\vec{n}, \qquad \vec{n} = (n_x, n_y, n_z), \tag{31}$$

where n_x, n_y, and n_z take natural numbers [91].

If the spatial lattice extent L is large enough, we can use approximate spherical symmetry and consider only the degenerate states [92]. Then the degeneracy of these states can be calculated by $C_3(n)$, where $n = n_x^2+n_y^2+n_z^2$.

Now using these definitions above, we rewrite the continuous integral in momentum space by

$$\int d^3\vec{l} \to \left(\frac{2\pi}{L}\right)^3 \sum_{n\in\mathbb{N}} C_3(n). \tag{32}$$

The loop integrals will be actually convergent when $n_{\max} > 75$.

C. The lattice spacing effect

We also examine the lattice spacing effect in this work. Following Refs. [93–95], we construct the concise Wilson matrix which is proportional to the lattice spacing a,

$$\rho_+ = \frac{1}{2} a(u^\dagger c_q u^\dagger + u c_q u), \tag{33}$$

where c_q denotes the Sheikholeslami-Wohlert coefficient matrix which reads $c_q = \mathrm{diag}(c_{sw}^u, c_{sw}^d, c_{sw}^s)$. The lattice QCD simulation used below gives $c_{sw}^{u/d,s} = 1.715$ [69]. The $\mathcal{O}(a)$ contributions can be canceled by incorporating the clover term into the lattice action [93,96].

We can construct the Lagrangian contributing to magnetic moments with the ρ_+ operator,

$$\begin{aligned}\mathcal{L}_{\rm int}^{\mathcal{O}(a^2)} &= b_1 m_B i\bar{B}[S^\mu, S^\nu]\hat{F}^+_{\mu\nu} B\mathrm{Tr}(\rho_+\rho_+) \\ &+ b_2 m_B i\bar{B}[S^\mu, S^\nu]\{\hat{F}^+_{\mu\nu}, \rho_+\} B\mathrm{Tr}(\rho_+) \\ &+ b_3 m_B i\bar{B}[S^\mu, S^\nu]\hat{F}^+_{\mu\nu}\rho_+\rho_+ B \\ &+ b_4 m_B i\bar{B}[S^\mu, S^\nu]\rho_+\hat{F}^+_{\mu\nu}\rho_+ B \\ &+ b_5 m_B i\bar{B}[S^\mu, S^\nu]\rho_+\rho_+\hat{F}^+_{\mu\nu} B. \end{aligned} \tag{34}$$

The spacing effects are equal for $\mu_{\Xi_{cc}^+}$ and $\mu_{\Omega_{cc}^+}$,

$$\begin{aligned}&\frac{e}{6} c_{sw}^2 a^2 m_B (12b_1 + 24b_2 + 4b_3 + 4b_4 + 4b_5) \\ &= \frac{e}{6} c_{sw}^2 a^2 m_B b, \end{aligned} \tag{35}$$

where b is the undetermined combined parameter.

D. Numerical results for magnetic moments

The magnetic moments are given at large pion masses in the lattice QCD simulations as shown in Fig. 2 [68,69]. To relate the kaon and pion masses, the following χPT relation is utilized [72,90,97]:

$$m_K^2 = \frac{1}{2} m_\pi^2 + \left(m_K^2 - \frac{1}{2} m_\pi^2\right)_{\rm phys}. \tag{36}$$

We use the lattice QCD masses in Refs. [68,69] for other hadrons.

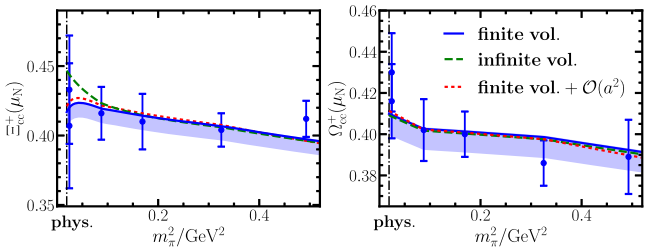

FIG. 2. Magnetic moments of Ξ_{cc}^+ and Ω_{cc}^+ as a function of m_π in units of μ_N. The lattice results are taken from Refs. [68,69] in $2+1$ flavor QCD, shown as the blue points. The green dashed and blue solid curves label our infinite and finite results, and the red dotted curves correspond to the scenario where both discrete momenta and $\mathcal{O}(a^2)$ are considered. The blue shaded regions illustrate the allowed probable range in our framework when we just fit the lattice results of $m_\pi = 0.296$, 0.411, 0.570 GeV.

We study these lattice QCD data and examine the finite volume and lattice spacing effects. We choose the cutoff with 0.7 GeV. Three scenarios of fits are given in Fig. 2, and the corresponding parameters are provided in Table III. From the left part of Fig. 2, one notices that the magnetic moment of Ξ_{cc}^+ near the physical pion mass seems to deviate a little from the dashed line without the finite-volume effect, which is why the χ^2 is big in the first line in Table III. After considering the finite-volume effect, the χ^2 decreases by about 15%. The finite-volume effect is important for interpreting the lattice QCD data.

The χ^2 is further reduced when the lattice spacing effect is also taken into account from Table III, but this effect is small. The parameter for the lattice spacing effect is fitted as

$$b = -0.07 \pm 0.23. \tag{37}$$

Its error is larger than the central value, which means the current accuracy in the lattice QCD simulations cannot effectively constrain the lattice spacing effect yet. The dotted and solid lines are also very close in Fig. 2. Therefore, in the following analysis the lattice spacing effect can be safely neglected.

For a more intuitive representation of the various loop-diagram contributions from different spin baryons, we illustrate the sizes of these contributions in Fig. 3. The loop-diagram contributions from spin-$\frac{3}{2}$ and spin-$\frac{1}{2}$ doubly charmed baryons exhibit different signs, which is because

TABLE III. The final fitting coupling constants in three cases.

	b	$-\frac{1}{3}a_1 + 4a_2$	χ^2
FRR	⋯	$1.61_{\pm 0.02}$	5.02
FRR + FV	⋯	$1.62_{\pm 0.02}$	4.30
FRR + FV + $\mathcal{O}(a^2)$	$-0.07_{\pm 0.23}$	$1.83_{\pm 0.68}$	4.20

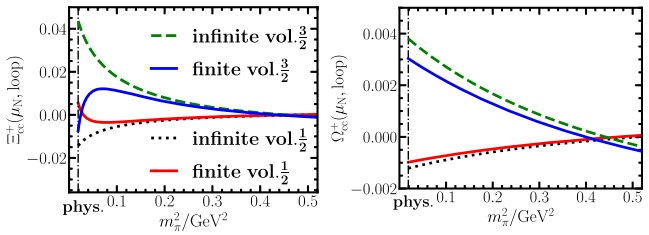

FIG. 3. Comparison between the loop contributions to the magnetic moments with the intermediate baryons as the $1/2$ and $3/2$ doubly charmed baryons.

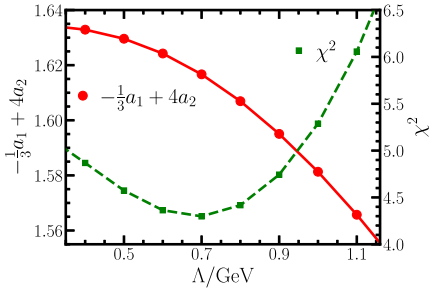

FIG. 4. The red dots represent the variation trend of tree-level coupling constants with cutoff, and the green dots are the magnitude of the corresponding χ^2 values. We connect data points with continuous lines for clarity.

the coefficients of them have opposite signs as in Table II. For the same reason, their magnitudes have an approximate ratio of 3:1 [98]. The graph shows that the main finite-volume correction lies in the chiral limit [99].

The dashed and solid lines exhibit an obvious deviation at small pion masses for the magnetic moment of Ξ_{cc}^{+} in Figs. 2 and 3, particularly when $m_\pi^2 < 0.1\ \text{GeV}^2$. If we drop the contribution from the loop momentum $\vec{l} = \vec{0}$ in the finite volume, the solid line would approach to the dashed line. The intermediate meson in Fig. 1 is pion for $\mu_{\Xi_{cc}^{+}}$ while it is kaon for $\mu_{\Omega_{cc}^{+}}$, which leads to no such phenomenon in the right part because the heavy mass of kaon suppresses the contribution in the finite volume.

The errors of lattice QCD data near the physical pion mass are relatively large, and the results at the largest pion mass may exceed the applicable range of ChPT extrapolation. Therefore, we refit the lattice data only with $m_\pi = 0.296$, 0.411, 0.570 GeV to check whether our results are stable or not. The blue shaded regions in Fig. 2 represent this new fit with $-\frac{1}{3}a_1 + 4a_2 = 1.60_{\pm 0.02}$ and $b = 0$. As we can see, the results do not change much.

The magnetic moments were studied with the dimensional regularization in Ref. [72], where the four $\mu_{\Xi_{cc}^{+}}$ at large pion masses on the lattice were fitted without the contributions of the excited doubly charmed baryons in Fig. 1(c) and that gave $\chi^2 = 9.77$. We find that χ^2 would become 98.37 after adding Fig. 1(c) with the dimensional regularization. However, for the same four data, the χ^2 is only 0.72 (1.30) without (with) Fig. 1(c) if using the finite-range regularization.

In Ref. [68], $\mu_{\Xi_{cc}^{++}}/\mu_N = 0.089(45)$ is also provided at $m_\pi = 0.156$ GeV. With the finite volume effect, we can then get $a_1 = -1.26_{\pm 0.17}$ and $a_2 = 0.30_{\pm 0.01}$ after adding this new datum.

In an effective field theory for low-energy QCD, the magnetic moment can be systematically expanded in powers of m_π^2, which can be roughly expressed as

$$\mu_B = c_0 + c_1 m_\pi^2 + + I_{m_\pi}^{(\text{loop})} + \cdots. \tag{38}$$

When regulating the loop integrals using the momentum-space cutoff, the loop integrals generate the obvious cutoff dependence. Taking $J(0)$ in Eq. (27) as an example, the Taylor expansion yields

$$-\frac{\Lambda}{16\pi} + \frac{m}{8\pi} - \frac{3m^2}{16\pi\Lambda} + \frac{m^3}{4\pi\Lambda^2} + \mathcal{O}(m^4). \tag{39}$$

However, the Λ variations of the loop diagrams can be absorbed by the redefinitions of the c_i terms from the tree diagrams in principle.

We refit the above magnetic moments from lattice QCD with different cutoffs. The variation of the coupling $-\frac{1}{3}a_1 + 4a_2$ is shown in Fig. 4. For sufficiently high cutoffs, the fitted coupling displays an approximately linear trend.

To investigate how the fitting quality varies with the cutoff Λ, we plot the χ^2 values as green dots in Fig. 4. For $\Lambda < 1.0$ GeV, the χ^2 is around 5 and the change is less than 1, which states the physical observables are insensitive to the choice of the cutoff in this region. However, for $\Lambda > 1.0$ GeV, the χ^2 increases significantly, indicating that the convergence of perturbation expansion becomes worse. Since our analysis is limited to one-loop order, incorporating higher-order loops may reduce the cutoff dependence. The optimal fit is achieved at $\Lambda = 0.7$ GeV, and thus we adopt this value for our calculations.

Next, we would like to estimate the effect of mass difference δ on the magnetic moment of spin-$\frac{1}{2}$ charmed baryon. In the above calculation, we fix the mass difference $\delta = 0.068$ GeV, which is determined by the lattice QCD data of doubly charmed baryon masses with $m_\pi = 0.156$ GeV, as the masses of spin-$\frac{3}{2}$ doubly charmed baryons have not been provided at large pion masses in lattice QCD. Note that the mass difference between $\frac{3}{2}^{+}$ Δ and $\frac{1}{2}^{+}$ nucleon is 0.27–0.33 GeV for pion mass less than 0.6 GeV [100], and it changes by about 20%. For the doubly charmed baryon, it contains less light quarks and thus the mass difference may vary less with different pion mass. Accordingly, in the following Fig. 5, we vary the value of δ as 20% respective to the central value $\delta = 0.068$ GeV and present the magnetic moment $\mu^{\Xi_{cc}^{+}}$ at $m_\pi = 0.411$ GeV. The slight change in the blue dashed

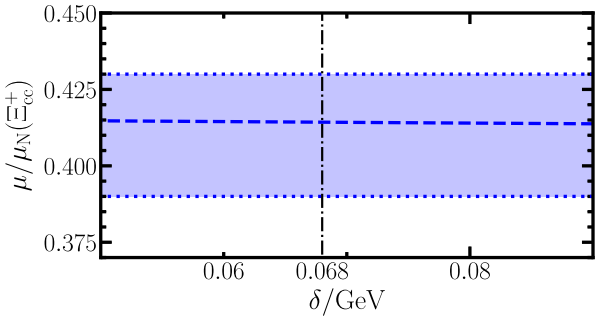

FIG. 5. The dependence of the magnetic moment $\mu^{\Xi_{cc}^+}$ at $m_\pi = 0.411$ GeV on δ, as indicated by the blue dashed line. The blue shaded region represents the error range of the lattice QCD data.

line indicates that the effect of mass difference is very small.

E. Magnetic form factors

To study the magnetic form factors, we need to consider the vector meson contribution as shown in Fig. 6 [73]. The Lagrangians involved are listed in Sec. II. The results can be expressed as

$$G_M^B(q^2) = g_V^B \frac{C_{VB}F_V}{m_V}\frac{q^2}{q^2 - m_V^2}. \tag{40}$$

Because of the significant breaking of SU(3) symmetry for the vector mesons, two couplings, $g_V^{\Xi_{cc}}$ and $g_V^{\Omega_{cc}}$, are introduced. The coefficients C_{VB} are listed in Table II of Ref. [73]. The above equation shows that the vector mesons do not contribute to G_M as $q^2 \to 0$, and that is why we do not mention them for the magnetic moments. The dependence of G_M can also be empirically parametrized as dipole form factor $G_M(Q^2) = G_M(0)/(1 + Q^2/0.71\,\mathrm{GeV}^2)^2$ [101–106].

In order to introduce the dependence of vector meson masses on m_π, we use [107]

$$\begin{aligned} m_\rho^2 &= m_\omega^2 = m_0^2 + 2\lambda_m m_\pi^2 + \lambda_0(2m_K^2 + m_\pi^2), \\ m_\phi^2 &= m_0^2 + 4\lambda_m m_K^2 - 2\lambda_m m_\pi^2 + \lambda_0(2m_K^2 + m_\pi^2), \end{aligned} \tag{41}$$

where $m_0 \approx 0.712$ GeV, $\lambda_m \approx 0.489$, and $\lambda_0 \approx 0.126$. There are also different pion mass dependences for them [108,109], but this discrepancy does not impact our ultimate conclusion.

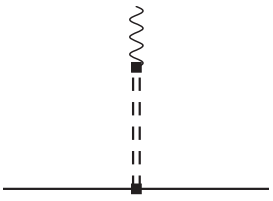

FIG. 6. The vector meson dominance diagram for the magnetic form factors of the doubly charmed baryons.

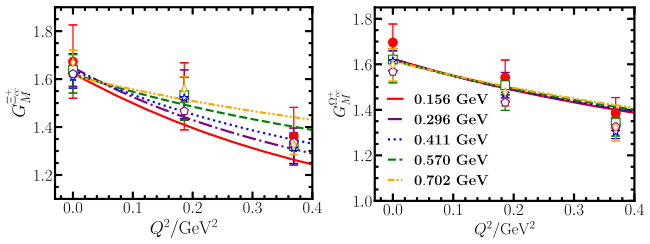

FIG. 7. Comparison between the magnetic form factors from the lattice QCD data and our results. The lattice QCD data are taken from Refs. [68,69]. The contributions of spin-$\frac{3}{2}$ baryons and the vector meson dominance model in the finite volume are considered.

We obtain the tree-level couplings by fitting the lattice QCD results from Tsukuba actions, where the pion mass is 156 MeV [68], as shown by the red points in Fig. 7. Both of the contributions from vector mesons and discrete-momentum effects are considered. The final results are $g_V^{\Xi_{cc}} = 7.95_{\pm 2.04}$ and $g_V^{\Omega_{cc}} = 22.84_{\pm 6.09}$.

These parameters are used to calculate the trend as Q^2 increases for the other pion masses in Fig. 7. The different pion masses exhibit almost identical dependence on Q^2 for Ω_{cc}^+, as the masses of c and s quarks do not change obviously in the lattice configurations for different pion masses. For Ξ_{cc}^+, the left part clearly shows that the slope decreases with the increasing pion mass.

After obtaining the g_V^B and tree-level couplings in Table III, we can calculate the mean square radius $\langle r_M^2 \rangle$ in the infinite volume at the physical pion mass. The values are 0.30 fm^2 for Ξ_{cc}^+ and 0.15 fm^2 for Ω_{cc}^+. They are about 1/3 of the $\langle r_M^2 \rangle_{\mathrm{nucleon}}$, similar to those with the extended on-mass-shell scheme in Ref. [73].

IV. THE TRANSITION MAGNETIC FORM FACTORS

The matrix elements of electromagnetic current between spin-$\frac{1}{2}$ and spin-$\frac{3}{2}$ baryons are defined as [68,110]

$$\langle \Psi^{*\rho}(p')|J_\mu|\Psi(p)\rangle = \sqrt{\frac{2}{3}} e \bar{u}^\rho(p') \mathcal{O}_{\rho\mu}(p', p) u(p). \tag{42}$$

In the framework of HBChPT, the tensor $\mathcal{O}_{\rho\mu}$ can be parametrized in three Lorentz invariant terms:

$$\begin{aligned} \mathcal{O}_{\rho\mu}(p', p) = {} & 2G_1(q_\rho S_\mu - q\cdot S g_{\rho\mu}) \\ & + G_2 \frac{2m_T}{m_B + m_T}(q_\rho v_\mu - q\cdot v g_{\rho\mu}) q\cdot S \\ & + G_3 \frac{2}{m_B + m_T}(q_\mu q_\rho - q^2 g_{\rho\mu}) q\cdot S. \end{aligned} \tag{43}$$

Here $u^\rho(p)$ is a spin vector in the Rarita-Schwinger formalism satisfying $v_\rho u^\rho(p) = 0$ and $\gamma_\rho u^\rho(p) = 0$ [85,111–114].

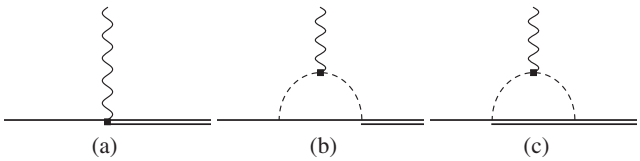

FIG. 8. Feynman diagrams for the transition magnetic moments.

The transition magnetic form factor $G_{M1}(q^2)$ is expressed as

$$G_{M1}(q^2) = \frac{m_B}{3(m_T+m_B)}\left[G_1\frac{(m_T+m_B)(3m_T+m_B)-q^2}{m_T} + G_2(m_T^2-m_B^2)+2q^2G_3\right]. \quad (44)$$

A. Expressions in the physical world

There are three Feynman diagrams that contribute to G_{M1} up to $\mathcal{O}(p^3)$, which are depicted in Fig. 8. The tree-level diagram comes from the Lagrangian in Eq. (9), while the baryon-meson vertex of the loop diagrams comes from the interaction Lagrangian in Eq. (14). The tree diagram only contributes to G_1 and can be expressed as

$$G_{M1}^{(2,\mathrm{tree})} = \gamma_B\sqrt{\frac{3}{2}}\frac{(m_T+m_B)(3m_T+m_B)-q^2}{3m_T(m_B+m_T)}. \quad (45)$$

The loop contributions are

$$G_{M1}^{(3,\mathrm{loop})} = G_{M1}^{(3,b)} + G_{M1}^{(3,c)}, \quad (46)$$

where

$$G_{M1}^{(3,b)} = \sqrt{\frac{3}{2}}\frac{m_B[(m_T+m_B)(3m_T+m_B)-q^2]}{6m_T(m_B+m_T)} \times\sum_{i=\pi,K}\left(\alpha_{AC}^{(i)}\frac{\tilde{g}_A\tilde{g}_C}{4f_i^2}\right)(n_3^{\mathrm{III}}+n_1^{\mathrm{II}}) + \sqrt{\frac{3}{2}}\frac{(m_T^2-m_B^2)m_B}{6m_T}\sum_{i=\pi,K}\left(\beta_{AC}^{(i)}\frac{\tilde{g}_A\tilde{g}_C}{4f_i^2}\right)(n_2^{\mathrm{III}}+n_4^{\mathrm{II}}) + \sqrt{\frac{3}{2}}\frac{m_Bq^2}{3}\sum_{i=\pi,K}\left(\zeta_{AC}^{(i)}\frac{\tilde{g}_A\tilde{g}_C}{4f_i^2}\right)(2n_1^{\mathrm{III}}+3n_2^{\mathrm{II}}+n_1^{\mathrm{I}}), \quad (47)$$

and

TABLE IV. The coefficients of the tree and loop correction to G_{M1} from Eqs. (45) and (47).

B	γ_B
Ξ_{cc}^{++}	$-\frac{1}{3}a_3-2a_4$
Ξ_{cc}^{+}	$\frac{1}{6}a_3-2a_4$
Ω_{cc}^{+}	$\frac{1}{6}a_3-2a_4$

B	$\alpha_{BC}^{(\pi)}$	$\alpha_{AC}^{(\pi)}$	$\alpha_{BC}^{(K)}$	$\alpha_{AC}^{(K)}$	$\beta_{BC}^{(\pi)}$	$\beta_{AC}^{(\pi)}$	$\beta_{BC}^{(K)}$	$\beta_{AC}^{(K)}$	$\zeta_{BC}^{(\pi)}$	$\zeta_{AC}^{(\pi)}$	$\zeta_{BC}^{(K)}$	$\zeta_{AC}^{(K)}$
Ξ_{cc}^{++}	$-\frac{2}{3}$	2	$-\frac{2}{3}$	2	$-\frac{2}{3}$	2	$-\frac{2}{3}$	2	$-\frac{1}{3}$	1	$-\frac{1}{3}$	1
Ξ_{cc}^{+}	$\frac{2}{3}$	-2	0	0	$\frac{2}{3}$	-2	0	0	$\frac{1}{3}$	-1	0	0
Ω_{cc}^{+}	0	0	$\frac{2}{3}$	-2	0	0	$\frac{2}{3}$	-2	0	0	$\frac{1}{3}$	-1

$$G_{M1}^{(3,c)} = \sqrt{\frac{3}{2}}\frac{m_B[(m_T+m_B)(3m_T+m_B)-q^2]}{6m_T(m_B+m_T)} \times\sum_{i=\pi,K}\left(\alpha_{BC}^{(i)}\frac{\tilde{g}_B\tilde{g}_C}{4f_i^2}\right)(n_3^{\mathrm{III}}-2n_1^{\mathrm{II}}) + \sqrt{\frac{3}{2}}\frac{(m_T^2-m_B^2)m_B}{6m_T}\sum_{i=\pi,K}\left(\beta_{BC}^{(i)}\frac{\tilde{g}_B\tilde{g}_C}{4f_i^2}\right)(n_2^{\mathrm{III}}+n_4^{\mathrm{II}}) + \sqrt{\frac{3}{2}}\frac{m_Bq^2}{3}\sum_{i=\pi,K}\left(\zeta_{BC}^{(i)}\frac{\tilde{g}_B\tilde{g}_C}{4f_i^2}\right)(2n_1^{\mathrm{III}}+3n_2^{\mathrm{II}}+n_1^{\mathrm{I}}). \quad (48)$$

We summarize the coefficients γ_B, $\alpha_{AC}^{(i)}$ $\alpha_{BC}^{(i)}$, $\beta_{AC}^{(i)}$, $\beta_{BC}^{(i)}$, $\zeta_{AC}^{(i)}$, and $\zeta_{BC}^{(i)}$ in Table IV. The forms of n_1^{I}, n_1^{II}, n_2^{II}, n_4^{II}, n_1^{III}, n_2^{III}, and n_3^{III} are also obtained by solving the Lorentzian invariant structures in the Appendix, which have been evaluated in the rest frame of the spin-$\frac{3}{2}$ baryon [77,80].

The method of deriving loop integrals is universally applicable, and it has been described in detail in the Appendix of Ref. [115]. The results conform to the following relationship:

$$2(n_1^{\mathrm{II}}+n_3^{\mathrm{III}})+2(n_2^{\mathrm{III}}+n_4^{\mathrm{II}})q\cdot v+(2n_1^{\mathrm{III}}+3n_2^{\mathrm{II}}+n_1^{\mathrm{I}})q^2 = -2n_3^{\mathrm{III}}, \quad (49)$$

and this ensures that the numerical matrix elements of electromagnetic current still have the tensor $\mathcal{O}_{\rho\mu}$ structure which can be obtained with the symmetry analysis.

Similarly, we consider the vector meson contribution as shown in Fig. 9 [56,57,73]. The specific Lagrangians of the interaction are provided in Eqs. (11) and (16). It only contributes through G_1 as

$$G_{M1}^{(\mathrm{vec.})} = \xi_V\frac{d_V^{\Xi_{cc}/\Omega_{cc}}F_V}{4\sqrt{2}m_V}\frac{q^2}{q^2-m_V^2} \times\frac{(m_T+m_B)(3m_T+m_B)-q^2}{m_T(m_B+m_T)}, \quad (50)$$

where the ξ_V values are listed in Table V.

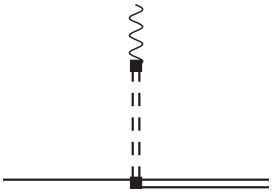

FIG. 9. The vector meson dominance diagram for the transition magnetic form factors.

B. Numerical results

The lattice QCD simulations provided the multipole form factors of doubly charmed baryons at $m_\pi = 0.156$ GeV and the transfer momentum square $Q^2 = -q^2 \approx 0.18$ GeV^2 with the spatial lattice extent $L = 2.9$ fm in Refs. [70,71], and we present them in Fig. 10. We explicitly consider the mass splitting, $\delta \approx 68$ MeV, between spin-$\frac{1}{2}$ and spin-$\frac{3}{2}$ doubly charmed baryons from the lattice QCD results.

For the vector meson contributions, we utilize heavy quark symmetry to relate the TBV and BBV couplings as mentioned in the Appendix, and thus $d_V^{\Xi_{cc}} = g_V^{\Xi_{cc}} = 7.95_{\pm 2.04}$ and $d_V^{\Omega_{cc}} = g_V^{\Omega_{cc}} = 22.84_{\pm 6.09}$. Our numerical results are presented in Fig. 10 with $\Lambda = 0.7$ GeV. The blue lines represent the fit that includes the contributions of vector mesons for the finite-volume version, and the fitted parameters are listed in Table VI. We also plot the allowed regions of this fit as the blue shades. It clearly shows that the HBChPT with FRR can describe the lattice QCD results well.

We fix a_3 and a_4 as in Table VI, replace the sum of the discrete momenta with the integral of the continuous momenta for the loop diagrams, and obtain the green dotted lines corresponding to the results in the infinite volume. The large difference between the blue solid lines and the green dotted lines indicates that the finite-volume effect is obvious at the current stage.

To show the effect of the vector mesons, we turn them off by setting $d_V = 0$ and obtain the black dashed lines with a_i in Table VI. They deviate about 2σ from the lattice QCD center data, which states that the vector mesons are important for the transition form factors even at small $Q^2 = -q^2 \approx 0.18$ GeV^2. Even if we refit the lattice QCD data by adjusting a_i without the vector mesons, the best fit as shown by the red dash-dotted lines exhibits a little tension with the lattice QCD datum in the middle part of Fig. 10.

TABLE V. The coefficients ξ_V of vector meson contribution in Eq. (50).

	Ξ_{cc}^{++}	Ξ_{cc}^{+}	Ω_{cc}^{+}
ρ	$\frac{\sqrt{2}}{2}$	$-\frac{\sqrt{2}}{2}$	0
ω	$\frac{\sqrt{2}}{6}$	$\frac{\sqrt{2}}{6}$	0
ϕ	0	0	$-\frac{\sqrt{2}}{3}$

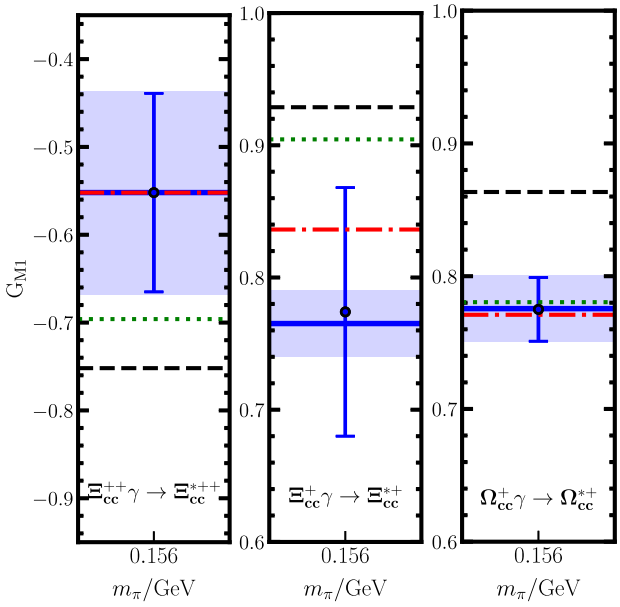

FIG. 10. The magnetic multipole transition form factors G_{M1} of doubly charmed baryons at $m_\pi = 0.156$ GeV and $Q^2 = -q^2 \approx 0.18$ GeV^2 with the spatial lattice extent $L = 2.9$ fm. With the corrections of vector mesons, the solid blue lines represent the results in the finite volume while the green dotted lines label our infinite-volume results. The black dashed lines label our finite-volume results for $d_V = 0$, that is, the vector meson contributions are turned off. The red dash-dotted lines represent the new fits by adjusting a_i with $d_V = 0$. The blue shaded regions illustrate the allowed ranges based on the fit within our framework. The lattice QCD data are taken from Ref. [70].

We separate the G_{M1} into four parts: the tree-level term and the loop terms proportional to G_1, G_2, and G_3. The tree diagram only itself will lead to zero for G_2 and G_3. Taking the Ω_{cc} case at $q^2 = -0.18$ GeV^2 and $m_\pi = 156$ MeV as an example,

$$G_{M1}^{\Omega_{cc}^+} = 0.756 + [0.019 + 0.001 - 0.002] = 0.774. \quad (51)$$

It is clear that the tree diagram dominates in our framework, and the loops give about 15% corrections.

The G_3 related term above is tiny and will be strictly 0 at $q^2 = 0$:

$$G_{M1}^{\Omega_{cc}^+}(q^2 = 0) = 0.843 + [0.065 - 0.062 + 0] = 0.846. \quad (52)$$

TABLE VI. The fitted couplings.

a_3	a_4
$1.83_{\pm 0.16}$	$-0.11_{\pm 0.01}$

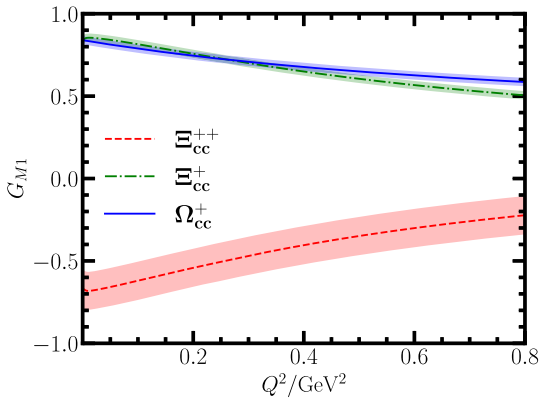

FIG. 11. Our predictions for the transition magnetic form factors G_{M1} as Q^2 increases with $m_\pi = 0.156$ GeV and $L = 2.9$ fm.

The third lines in Eqs. (47) and (48) correspond to the G_3 term and cancel themselves out as $q^2 \to 0$ due to the constraints from heavy quark symmetry on the couplings $\tilde{g}_A$, $\tilde{g}_B$, and $\tilde{g}_C$ which appear in the loop diagrams. However, with a slight breaking of heavy quark symmetry, for example, $\tilde{g}_A \to \tilde{g}_A$, $\tilde{g}_B \to 0.95\tilde{g}_B$, and $\tilde{g}_C \to \tilde{g}_C$, one has

$$q^2 G_3(q^2)|_{q^2\to 0} \neq 0, \tag{53}$$

and

$$G_{M1}^{\Omega_{cc}^+}(q^2 = 0) = 0.843 + [0.061 - 0.015 - 0.043] = 0.846. \tag{54}$$

If the static G_3 terms can be extracted accurately on the lattice, the breaking of the heavy quark symmetry would be understood better.

Finally, we predict the trend of G_{M1} in Fig. 11 at $m_\pi = 0.156$ GeV and $L = 2.9$ fm for the range $Q^2 =$ 0–0.8 GeV^2 with the fitting couplings in Table VI. From the figure, the $G_{M1}^{\Xi_{cc}^{++}}$ exhibits the opposite trend compared to the others. The main reason is that the contributions from the vector mesons have different signs for these transition form factors, which can be easily estimated from Table V. We hope they can be examined in the future.

V. SUMMARY

In this work, we employ HBChPT to study the magnetic form factors and transition magnetic form factors of the doubly charmed baryons up to $\mathcal{O}(p^3)$. The loop integrals are dealt with the finite-range regularization. We found that finite volume effects are important for interpreting the lattice QCD data, while the lattice spacing effect is not obvious compared to the current accuracy of simulation. We can simultaneously explain three different groups of the lattice QCD data very well as shown in Figs. 2, 7, and 10.

We consider both spin-$\frac{1}{2}$ and spin-$\frac{3}{2}$ doubly charmed baryons as the intermediate states in the loop diagrams. For the magnetic moments, the spin-$\frac{3}{2}$ loop contributions are relatively bigger and have different signs from the spin-$\frac{1}{2}$ ones.

The finite-volume effects improve the consistency of our results with lattice QCD data, particularly in the small pion-mass region. This improvement arises from the contribution of the zero-momentum mode ($\vec{l} = \vec{0}$) in finite volumes. In contrast, the finite-volume corrections for the Ω_{cc}^+ baryon are less pronounced, as the loops involve kaons which are less sensitive to these effects. For the magnetic form factors, the contributions from vector mesons are introduced to examine the q^2 dependence of G_M. These corrections become increasingly important as q^2 grows.

We have also studied the transition form factors G_{M1} for the processes $\Xi_{cc}^{++}\gamma \to \Xi_{cc}^{*++}$, $\Xi_{cc}^{+}\gamma \to \Xi_{cc}^{*+}$, and $\Omega_{cc}^{+}\gamma \to \Omega_{cc}^{*+}$. The finite-volume effects are also significant for the transition magnetic form factors when fitting to the lattice QCD results. The vector mesons play a crucial role in the transition form factors, even at small momentum transfer, $Q^2 = -q^2 \approx 0.18$ GeV^2. We carefully examine the loop contributions associated with the G_1, G_2, and G_3 terms, and the G_3 terms becomes bigger if the heavy quark symmetry is not strictly kept. Furthermore, we provide predictions for the transition form factors as a function of Q^2.

We have systematically studied the electromagnetic properties of the doubly charmed baryons within HBChPT, which can also help us understand the nonperturbative strong interactions. We expect our study can be further confirmed in the future lattice QCD calculations or experiments.

ACKNOWLEDGMENTS

This project is supported by the National Natural Science Foundation of China under Grants No. 12175091, No. 12335001, and No. 12247101, the Fundamental Research Funds for the Central Universities under Grant No. lzujbky-2024-jdzx06, the Natural Science Foundation of Gansu Province under Grants No. 22JR5RA389 and No. 25JRRA799, the "111 Center" under Grant No. B20063, and the Innovation Project for Young Science and Technology Talents of Lanzhou city under Grant No. 2023-QN-107.

DATA AVAILABILITY

The data that support the findings of this article are openly available [67,68,70].

APPENDIX: LOOP INTEGRALS

We collect some common loop functions as follows [82,115,116]:

$$\Delta = i\int \frac{d^4 l}{(2\pi)^4}\frac{1}{l^2 - m^2 + i\epsilon}, \tag{A1}$$

$$I_0(q^2) = i\int \frac{d^4l}{(2\pi)^4}\frac{1}{(l^2-m^2+i\epsilon)[(l+q)^2-m^2+i\epsilon]}, \tag{A2}$$

$$J_0(\omega) = i\int \frac{d^4l}{(2\pi)^4}\frac{1}{(l^2-m^2+i\epsilon)(v\cdot l+\omega+i\epsilon)}, \tag{A3}$$

$$\begin{aligned} &i\int \frac{d^4l}{(2\pi)^4}\frac{[1, l_\alpha, l_\alpha l_\beta, l_\nu l_\alpha l_\beta]}{(l^2-m^2+i\epsilon)[(l+q)^2-m^2+i\epsilon](v\cdot l+\omega+i\epsilon)} \\ &= [L_0(\omega), L_\alpha, L_{\alpha\beta}, L_{\nu\alpha\beta}], \end{aligned} \tag{A4}$$

where

$$\begin{aligned} L_\alpha &= n_1^{\mathrm{I}} q_\alpha + n_2^{\mathrm{I}} v_\alpha, \\ L_{\alpha\beta} &= n_1^{\mathrm{II}} g_{\alpha\beta} + n_2^{\mathrm{II}} q_\alpha q_\beta + n_3^{\mathrm{II}} v_\alpha v_\beta + n_4^{\mathrm{II}}(v_\alpha q_\beta + q_\alpha v_\beta), \\ L_{\nu\alpha\beta} &= n_1^{\mathrm{III}} q_\nu q_\alpha q_\beta + n_2^{\mathrm{III}}(q_\nu q_\alpha v_\beta + q_\nu q_\beta v_\alpha + q_\alpha q_\beta v_\nu) \\ &\quad + n_3^{\mathrm{III}}(q_\nu g_{\alpha\beta} + q_\beta g_{\nu\alpha} + q_\alpha g_{\nu\beta}) \\ &\quad + n_4^{\mathrm{III}}(q_\nu v_\alpha v_\beta + q_\alpha v_\nu v_\beta + q_\beta v_\nu v_\alpha) \\ &\quad + n_5^{\mathrm{III}}(g_{\nu\beta} v_\alpha + g_{\nu\alpha} v_\beta + g_{\alpha\beta} v_\nu) + n_6^{\mathrm{III}} v_\nu v_\alpha v_\beta. \end{aligned}$$

[1] A. Ocherashvili *et al.* (SELEX Collaboration), Confirmation of the double charm baryon $\Xi_{cc}^+(3520)$ via its decay to pD^+K^-, Phys. Lett. B **628**, 18 (2005).

[2] R. Aaij *et al.* (LHCb Collaboration), Precision measurement of the Ξ_{cc}^{++} mass, J. High Energy Phys. 02 (2020) 049.

[3] R. Aaij *et al.* (LHCb Collaboration), First observation of the doubly charmed baryon decay $\Xi_{cc}^{++} \to \Xi_c^+\pi^+$, Phys. Rev. Lett. **121**, 162002 (2018).

[4] S. P. Ratti, New results on c-baryons and a search for cc-baryons in FOCUS, Nucl. Phys. B, Proc. Suppl. **115**, 33 (2003).

[5] B. Aubert *et al.* (*BABAR* Collaboration), Search for doubly charmed baryons Ξ_{cc}^+ and Ξ_{cc}^{++} in *BABAR*, Phys. Rev. D **74**, 011103 (2006).

[6] R. Aaij *et al.* (LHCb Collaboration), Search for the doubly charmed baryon Ξ_{cc}^+ in the $\Xi_c^+\pi^-\pi^+$ final state, J. High Energy Phys. 12 (2021) 107.

[7] R. Chistov *et al.* (Belle Collaboration), Observation of new states decaying into $\Lambda_c^+K^-\pi^+$ and $\Lambda_c^+K_S^0\pi^-$, Phys. Rev. Lett. **97**, 162001 (2006).

[8] R. Aaij *et al.* (LHCb Collaboration), Measurement of the lifetime of the doubly charmed baryon Ξ_{cc}^{++}, Phys. Rev. Lett. **121**, 052002 (2018).

[9] R. Aaij *et al.* (LHCb Collaboration), Measurement of Ξ_{cc}^{++} production in pp collisions at $\sqrt{s} = 13$ TeV, Chin. Phys. C **44**, 022001 (2020).

[10] R. Aaij *et al.* (LHCb Collaboration), Observation of the doubly charmed baryon decay $\Xi_{cc}^{++} \to \Xi_c'^+\pi^+$, J. High Energy Phys. 05 (2022) 038.

[11] R. Aaij *et al.* (LHCb Collaboration), A search for $\Xi_{cc}^{++} \to D^+pK^-\pi^+$ decays, J. High Energy Phys. 10 (2019) 124.

[12] R. Aaij *et al.* (LHCb Collaboration), Search for the doubly charmed baryon Ω_{cc}^+, Sci. China Phys. Mech. Astron. **64**, 101062 (2021).

[13] M. Mattson *et al.* (SELEX Collaboration), First observation of the doubly charmed baryon Ξ_{cc}^+, Phys. Rev. Lett. **89**, 112001 (2002).

[14] R. Aaij *et al.* (LHCb Collaboration), Observation of the doubly charmed baryon Ξ_{cc}^{++}, Phys. Rev. Lett. **119**, 112001 (2017).

[15] Z. G. Wang, Analysis of the doubly heavy baryon states and pentaquark states with QCD sum rules, Eur. Phys. J. C **78**, 826 (2018).

[16] G. L. Yu, Z. Y. Li, Z. G. Wang, J. Lu, and M. Yan, Systematic analysis of doubly charmed baryons Ξ_{cc} and Ω_{cc}, Eur. Phys. J. A **59**, 126 (2023).

[17] M. Shekari Tousi and K. Azizi, Properties of doubly heavy spin-12 baryons: The ground and excited states, Phys. Rev. D **109**, 054005 (2024).

[18] T. M. Aliev, K. Azizi, and M. Savci, Doubly heavy spin–1/2 baryon spectrum in QCD, Nucl. Phys. **A895**, 59 (2012).

[19] T. M. Aliev, K. Azizi, and M. Savci, The masses and residues of doubly heavy spin-3/2 baryons, J. Phys. G **40**, 065003 (2013).

[20] Z. G. Wang, Analysis of the $1/2^-$ and $3/2^-$ heavy and doubly heavy baryon states with QCD sum rules, Eur. Phys. J. A **47**, 81 (2011).

[21] W. F. Wang, A. Feijoo, J. Song, and E. Oset, Molecular Ω_{cc}, Ω_{bb}, and Ω_{bc} states, Phys. Rev. D **106**, 116004 (2022).

[22] D. L. Yao, Masses and sigma terms of doubly charmed baryons up to $\mathcal{O}(p^4)$ in manifestly Lorentz-invariant baryon chiral perturbation theory, Phys. Rev. D **97**, 034012 (2018).

[23] D. B. Lichtenberg, Magnetic moments of charmed baryons in the quark model, Phys. Rev. D **15**, 345 (1977).

[24] B. Julia-Diaz and D. O. Riska, Baryon magnetic moments in relativistic quark models, Nucl. Phys. **A739**, 69 (2004).

[25] A. Faessler, T. Gutsche, M. A. Ivanov, J. G. Korner, V. E. Lyubovitskij, D. Nicmorus, and K. Pumsa-ard, Magnetic moments of heavy baryons in the relativistic three-quark model, Phys. Rev. D **73**, 094013 (2006).

[26] S. N. Jena and D. P. Rath, Magnetic moments of light, charmed and *B* flavored baryons in a relativistic logarithmic potential, Phys. Rev. D **34**, 196 (1986).

[27] B. Patel, A. K. Rai, and P. C. Vinodkumar, Masses and magnetic moments of charmed baryons using hyper central model, arXiv:0803.0221.

[28] C. Albertus, E. Hernandez, J. Nieves, and J. M. Verde-Velasco, Static properties and semileptonic decays of

doubly heavy baryons in a nonrelativistic quark model, Eur. Phys. J. A **32**, 183 (2007); **36**, 119(E) (2008).
[29] Z. Shah, A. Kakadiya, K. Gandhi, and A. K. Rai, Properties of doubly heavy baryons, Universe **7**, 337 (2021).
[30] B. J. Lai, F. L. Wang, and X. Liu, Investigating the M1 radiative decay behaviors and the magnetic moments of the predicted triple-charm molecular-type pentaquarks, Phys. Rev. D **109**, 054036 (2024).
[31] R. Patel and M. Shah, Magnetic moment and decay properties of Ξ_{cc}^{++} baryon in relativistic Dirac formalism with independent quark model, DAE Symp. Nucl. Phys. **67**, 947 (2024).
[32] N. Sharma, H. Dahiya, P. K. Chatley, and M. Gupta, Spin $\frac{1}{2}^+$, spin $\frac{3}{2}^+$ and transition magnetic moments of low lying and charmed baryons, Phys. Rev. D **81**, 073001 (2010).
[33] Z. Shah and A. K. Rai, Excited state mass spectra of doubly heavy Ξ baryons, Eur. Phys. J. C **77**, 129 (2017).
[34] A. Majethiya, B. Patel, A. K. Rai, and P. C. Vinodkumar, Properties of doubly charmed baryons in the quark-diquark model, arXiv:0809.4910.
[35] B. Silvestre-Brac, Spectrum and static properties of heavy baryons, Few-Body Syst. **20**, 1 (1996).
[36] H. Mutuk, The status of Ξ_{cc}^{++} baryon: Investigating quark–diquark model, Eur. Phys. J. Plus **137**, 10 (2022).
[37] M. Shah, R. Patel, and P. C. Vinodkumar, Radial excitation of Ω_{cc} baryon using relativistic formalism, Few-Body Syst. **64**, 34 (2023).
[38] Z. Shah, K. Thakkar, and A. K. Rai, Excited state mass spectra of doubly heavy baryons Ω_{cc}, Ω_{bb} and Ω_{bc}, Eur. Phys. J. C **76**, 530 (2016).
[39] N. Barik and M. Das, Magnetic moments of confined quark and baryons in an independent quark model based on Dirac quark with power law potential, Phys. Rev. D **28**, 2823 (1983).
[40] H. Dahiya, N. Sharma, and P. K. Chatley, Magnetic moments of spin $\frac{1}{2}^+$ and spin $\frac{3}{2}^+$ charmed baryons, AIP Conf. Proc. **1257**, 395 (2010).
[41] S. Rahmani, H. Hassanabadi, and H. Sobhani, Mass and decay properties of double heavy baryons with a phenomenological potential model, Eur. Phys. J. C **80**, 312 (2020).
[42] A. Bernotas and V. Simonis, Magnetic moments of heavy baryons in the bag model reexamined, arXiv:1209.2900.
[43] S. K. Bose and L. P. Singh, Magnetic moments of charmed and B flavored hadrons in MIT bag model, Phys. Rev. D **22**, 773 (1980).
[44] V. Simonis, Improved predictions for magnetic moments and M1 decay widths of heavy hadrons, arXiv:1803.01809.
[45] W. X. Zhang, H. Xu, and D. Jia, Masses and magnetic moments of hadrons with one and two open heavy quarks: Heavy baryons and tetraquarks, Phys. Rev. D **104**, 114011 (2021).
[46] Y. s. Oh, D. P. Min, M. Rho, and N. N. Scoccola, Massive quark baryons as skyrmions: Magnetic moments, Nucl. Phys. **A534**, 493 (1991).
[47] U. Özdem, Magnetic moments of doubly heavy baryons in light-cone QCD, J. Phys. G **46**, 035003 (2019).
[48] R. Dhir and R. C. Verma, Magnetic moments of $(J^P = 3/2^+)$ heavy baryons using effective mass scheme, Eur. Phys. J. A **42**, 243 (2009).
[49] B. Mohan, T. M. S., A. Hazra, and R. Dhir, Screening of the quark charge and mixing effects on transition moments and M1 decay widths of baryons, Phys. Rev. D **106**, 113007 (2022).
[50] A. Hazra, S. Rakshit, and R. Dhir, Radiative M1 transitions of heavy baryons: Effective quark mass scheme, Phys. Rev. D **104**, 053002 (2021).
[51] S. Kumar, R. Dhir, and R. C. Verma, Magnetic moments of charm baryons using effective mass and screened charge of quarks, J. Phys. G **31**, 141 (2005).
[52] A. N. Gadaria, N. R. Soni, and J. N. Pandya, Masses and magnetic moment of doubly heavy baryons, DAE Symp. Nucl. Phys. **61**, 698 (2016).
[53] R. H. Hackman, N. G. Deshpande, D. A. Dicus, and V. L. Teplitz, M1 transitions in the MIT bag model, Phys. Rev. D **18**, 2537 (1978).
[54] A. Bernotas and V. Šimonis, Radiative M1 transitions of heavy baryons in the bag model, Phys. Rev. D **87**, 074016 (2013).
[55] E.-L. Cui, H.-X. Chen, W. Chen, X. Liu, and S.-L. Zhu, Suggested search for doubly charmed baryons of $J^P = 3/2^+$ via their electromagnetic transitions, Phys. Rev. D **97**, 034018 (2018).
[56] T. M. Aliev, T. Barakat, and K. Şimşek, Strong $B^*_{QQ'}B_{QQ'}V$ vertices and the radiative decays of $B^*_{QQ} \to B_{QQ}\gamma$ in the light-cone sum rules, Eur. Phys. J. A **57**, 160 (2021).
[57] T. Aliyev and S. Bilmiş, Properties of doubly heavy baryons in QCD, Turk. J. Phys. **46**, 1 (2022).
[58] T. M. Aliev, E. Askan, and A. Ozpineci, Radiative decays of the spin-3/2 to spin-1/2 doubly heavy baryons in QCD, Phys. Rev. D **108**, 054015 (2023).
[59] N. Soni and J. Pandya, Masses and radiative decay of Ω_{cc}^+ baryon, DAE Symp. Nucl. Phys. **62**, 770 (2017).
[60] A. N. Gadaria, N. R. Soni, R. Chaturvedi, A. Kumar Rai, and J. N. Pandya, Decay properties of Ξ_{cc}^{++} baryon, DAE Symp. Nucl. Phys. **63**, 912 (2018).
[61] Q. F. Lü, K. L. Wang, L. Y. Xiao, and X. H. Zhong, Mass spectra and radiative transitions of doubly heavy baryons in a relativized quark model, Phys. Rev. D **96**, 114006 (2017).
[62] T. Branz, A. Faessler, T. Gutsche, M. A. Ivanov, J. G. Korner, V. E. Lyubovitskij, and B. Oexl, Radiative decays of double heavy baryons in a relativistic constituent three–quark model including hyperfine mixing, Phys. Rev. D **81**, 114036 (2010).
[63] L. Y. Xiao, K. L. Wang, Q. f. Lu, X. H. Zhong, and S. L. Zhu, Strong and radiative decays of the doubly charmed baryons, Phys. Rev. D **96**, 094005 (2017).
[64] H. S. Li, L. Meng, Z. W. Liu, and S. L. Zhu, Radiative decays of the doubly charmed baryons in chiral perturbation theory, Phys. Lett. B **777**, 169 (2018).
[65] H. S. Li, L. Meng, Z. W. Liu, and S. L. Zhu, Magnetic moments of the doubly charmed and bottom baryons, Phys. Rev. D **96**, 076011 (2017).
[66] H. S. Li and W. L. Yang, Spin-$\frac{3}{2}$ doubly charmed baryon contribution to the magnetic moments of the spin-$\frac{1}{2}$ doubly charmed baryons, Phys. Rev. D **103**, 056024 (2021).
[67] K. U. Can, G. Erkol, B. Isildak, M. Oka, and T. T. Takahashi, Electromagnetic structure of charmed baryons in lattice QCD, J. High Energy Phys. 05 (2014) 125.

[68] H. Bahtiyar, Electromagnetic structure of spin-12 doubly charmed baryons in lattice QCD, Phys. Rev. D **108**, 034504 (2023).

[69] K. U. Can, Lattice QCD study of the elastic and transition form factors of charmed baryons, Int. J. Mod. Phys. A **36**, 2130013 (2021).

[70] H. Bahtiyar, K. U. Can, G. Erkol, M. Oka, and T. T. Takahashi, Radiative transitions of doubly charmed baryons in lattice QCD, Phys. Rev. D **98**, 114505 (2018).

[71] H. Bahtiyar, K. U. Can, G. Erkol, M. Oka, and T. T. Takahashi, Radiative transitions of singly and doubly charmed baryons in lattice QCD, J. Phys. Soc. Jpn. Conf. Proc. **26**, 022027 (2019).

[72] M. Z. Liu, Y. Xiao, and L. S. Geng, Magnetic moments of the spin-$1/2$ doubly charmed baryons in covariant baryon chiral perturbation theory, Phys. Rev. D **98**, 014040 (2018).

[73] A. N. Hiller Blin, Z. F. Sun, and M. J. Vicente Vacas, Electromagnetic form factors of spin $1/2$ doubly charmed baryons, Phys. Rev. D **98**, 054025 (2018).

[74] J. F. Donoghue and B. R. Holstein, Improved treatment of loop diagrams in SU(3) baryon chiral perturbation theory, Phys. Lett. B **436**, 331 (1998).

[75] J. F. Donoghue, B. R. Holstein, and B. Borasoy, SU(3) baryon chiral perturbation theory and long distance regularization, Phys. Rev. D **59**, 036002 (1999).

[76] G. J. Wang, L. Meng, and S. L. Zhu, Radiative decays of the singly heavy baryons in chiral perturbation theory, Phys. Rev. D **99**, 034021 (2019).

[77] G. C. Gellas, T. R. Hemmert, C. N. Ktorides, and G. I. Poulis, The Delta nucleon transition form-factors in chiral perturbation theory, Phys. Rev. D **60**, 054022 (1999).

[78] T. A. Gail and T. R. Hemmert, Signatures of chiral dynamics in the nucleon to delta transition, Eur. Phys. J. A **28**, 91 (2006).

[79] A. Faessler, T. Gutsche, B. R. Holstein, V. E. Lyubovitskij, D. Nicmorus, and K. Pumsa-ard, Light baryon magnetic moments and $N \to \Delta\gamma$ transition in a Lorentz covariant chiral quark approach, Phys. Rev. D **74**, 074010 (2006).

[80] D. Arndt and B. C. Tiburzi, Baryon decuplet to octet electromagnetic transitions in quenched and partially quenched chiral perturbation theory, Phys. Rev. D **69**, 014501 (2004).

[81] H. S. Li, Z. W. Liu, X. L. Chen, W. Z. Deng, and S. L. Zhu, Decuplet to octet baryon transitions in chiral perturbation theory, Eur. Phys. J. C **79**, 66 (2019).

[82] S. Scherer, Introduction to chiral perturbation theory, Adv. Nucl. Phys. **27**, 277 (2003).

[83] Z. R. Liang, P. C. Qiu, and D. L. Yao, One-loop analysis of the interactions between doubly charmed baryons and Nambu-Goldstone bosons, J. High Energy Phys. 07 (2023) 124.

[84] P. C. Qiu and D. L. Yao, Chiral effective Lagrangian for doubly charmed baryons up to $\mathcal{O}(q^4)$, Phys. Rev. D **103**, 034006 (2021).

[85] W. Rarita and J. Schwinger, On a theory of particles with half integral spin, Phys. Rev. **60**, 61 (1941).

[86] B. Borasoy and U. G. Meissner, Chiral Lagrangians for baryons coupled to massive spin 1 fields, Int. J. Mod. Phys. A **11**, 5183 (1996).

[87] A. F. Falk, Hadrons of arbitrary spin in the heavy quark effective theory, Nucl. Phys. **B378**, 79 (1992).

[88] L. Meng and S. L. Zhu, Light pseudoscalar meson and doubly charmed baryon scattering lengths with heavy diquark-antiquark symmetry, Phys. Rev. D **100**, 014006 (2019).

[89] Z. F. Sun and M. J. Vicente Vacas, Masses of doubly charmed baryons in the extended on-mass-shell renormalization scheme, Phys. Rev. D **93**, 094002 (2016).

[90] I. C. Cloet, D. B. Leinweber, and A. W. Thomas, Delta baryon magnetic moments from lattice QCD, Phys. Lett. B **563**, 157 (2003).

[91] Z. R. Liang and D. L. Yao, A unified formulation of one-loop tensor integrals for finite volume effects, J. High Energy Phys. 12 (2022) 029.

[92] Y. Li, J. J. Wu, C. D. Abell, D. B. Leinweber, and A. W. Thomas, Partial wave mixing in Hamiltonian effective field theory, Phys. Rev. D **101**, 114501 (2020).

[93] X. L. Ren, L. S. Geng, and J. Meng, Baryon chiral perturbation theory with Wilson fermions up to $\mathcal{O}(a^2)$ and discretization effects of latest $n_f = 2 + 1$ LQCD octet baryon masses, Eur. Phys. J. C **74**, 2754 (2014).

[94] B. C. Tiburzi, Baryon masses at $O(a^2)$ in chiral perturbation theory, Nucl. Phys. **A761**, 232 (2005).

[95] D. Arndt and B. C. Tiburzi, Hadronic electromagnetic properties at finite lattice spacing, Phys. Rev. D **69**, 114503 (2004).

[96] O. Bar, G. Rupak, and N. Shoresh, Chiral perturbation theory at $O(a^2)$ for lattice QCD, Phys. Rev. D **70**, 034508 (2004).

[97] P. Wang, D. B. Leinweber, A. W. Thomas, and R. D. Young, Chiral extrapolation of octet-baryon charge radii, Phys. Rev. D **79**, 094001 (2009).

[98] Z. W. Liu and S. L. Zhu, Pseudoscalar meson and charmed baryon scattering lengths, Phys. Rev. D **86**, 034009 (2012); **93**, 019901(E) (2016).

[99] R. D. Young, D. B. Leinweber, and A. W. Thomas, Leading quenching effects in the proton magnetic moment, Phys. Rev. D **71**, 014001 (2005).

[100] S. Aoki *et al.* (PACS-CS Collaboration), $2 + 1$ flavor lattice QCD toward the physical point, Phys. Rev. D **79**, 034503 (2009).

[101] P. Wang, D. B. Leinweber, A. W. Thomas, and R. D. Young, Chiral extrapolation of nucleon magnetic form factors, Phys. Rev. D **75**, 073012 (2007).

[102] C. F. Perdrisat, V. Punjabi, and M. Vanderhaeghen, Nucleon electromagnetic form factors, Prog. Part. Nucl. Phys. **59**, 694 (2007).

[103] P. Mergell, U. G. Meissner, and D. Drechsel, Dispersion theoretical analysis of the nucleon electromagnetic form-factors, Nucl. Phys. **A596**, 367 (1996).

[104] B. Kubis and U. G. Meissner, Low-energy analysis of the nucleon electromagnetic form-factors, Nucl. Phys. **A679**, 698 (2001).

[105] B. Kubis and U. G. Meissner, Baryon form-factors in chiral perturbation theory, Eur. Phys. J. C **18**, 747 (2001).

[106] A. N. Hiller Blin, Systematic study of octet-baryon electromagnetic form factors in covariant chiral perturbation theory, Phys. Rev. D **96**, 093008 (2017).

[107] Y. Zhou, X. L. Ren, H. X. Chen, and L. S. Geng, Pseudoscalar meson and vector meson interactions and dynamically generated axial-vector mesons, Phys. Rev. D **90**, 014020 (2014).
[108] I. V. Danilkin, L. I. R. Gil, and M. F. M. Lutz, Dynamical light vector mesons in low-energy scattering of Goldstone bosons, Phys. Lett. B **703**, 504 (2011).
[109] X. L. Ren, Light-quark mass dependence of the $\Lambda(1405)$ resonance, Phys. Lett. B **855**, 138802 (2024).
[110] H. F. Jones and M. D. Scadron, Multipole $\gamma N\Delta$ formfactors and resonant photoproduction and electroproduction, Ann. Phys. (N.Y.) **81**, 1 (1973).
[111] S. Nozawa and D. B. Leinweber, Electromagnetic formfactors of spin $3/2$ baryons, Phys. Rev. D **42**, 3567 (1990).
[112] T. R. Hemmert, Heavy baryon chiral perturbation theory with light deltas, Report No. UMI-98-09346, University of Massachusetts, 1997.
[113] T. R. Hemmert, B. R. Holstein, and J. Kambor, Systematic 1/M expansion for spin $3/2$ particles in baryon chiral perturbation theory, Phys. Lett. B **395**, 89 (1997).
[114] E. E. Jenkins and A. V. Manohar, Chiral corrections to the baryon axial currents, Phys. Lett. B **259**, 353 (1991).
[115] L. Meng, B. Wang, G. J. Wang, and S. L. Zhu, The hidden charm pentaquark states and $\Sigma_c\bar{D}^{(*)}$. interaction in chiral perturbation theory, Phys. Rev. D **100**, 014031 (2019).
[116] B. Wang, Z. W. Liu, and X. Liu, $\bar{B}^{(*)}.\bar{B}^{(*)}$. Interactions in chiral effective field theory, Phys. Rev. D **99**, 036007 (2019).